Room-Temperature High-Frequency Transport of Dirac Fermions in Epitaxially Grown Sb_2Te_3- and Bi_2Te_3-Based Topological Insulators

P. Olbrich,[1] L. E. Golub,[2] T. Herrmann,[1] S. N. Danilov,[1] H. Plank,[1] V. V. Bel'kov,[2] G. Mussler,[3] Ch. Weyrich,[3] C. M. Schneider,[3] J. Kampmeier,[3] D. Grützmacher,[3] L. Plucinski,[3] M. Eschbach,[3] and S. D. Ganichev[1]

[1]*Terahertz Center, University of Regensburg, 93040 Regensburg, Germany*
[2]*Ioffe Physical-Technical Institute, 194021 St. Petersburg, Russia*
[3]*Jülich Aachen Research Alliance (JARA-FIT), Leo Brandt Straße, 52425 Jülich, Germany*

(Received 28 February 2014; revised manuscript received 25 April 2014; published 25 August 2014)

We report on the observation of photogalvanic effects in epitaxially grown Sb_2Te_3 and Bi_2Te_3 three-dimensional (3D) topological insulators (TI). We show that asymmetric scattering of Dirac fermions driven back and forth by the terahertz electric field results in a dc electric current. Because of the "symmetry filtration" the dc current is generated by the surface electrons only and provides an optoelectronic access to probe the electron transport in TI, surface domains orientation, and details of electron scattering in 3D TI even at room temperature.

DOI: 10.1103/PhysRevLett.113.096601 PACS numbers: 72.40.+w, 72.20.-i, 79.60.Bm, 85.75.-d

A new state of matter called the topological insulator has recently been theoretically predicted and experimentally observed in a number of materials, such as Bi_2Se_3, Sb_2Te_3, and Bi_2Te_3, for reviews, see [1–3]. The main feature of topological insulators (TI) emerges from its band structure. While the bulk of TI is an insulator with an inverted band structure, its surface hosts gapless states with a linear energy dispersion. Thus, carriers at the surface of TI are expected to have unique properties, such as extremely high mobilities or a spin-locked transport behavior, and are of potential interest for applications in the field of spintronics, optoelectronics, or quantum computing. Hence, a fabrication of TI materials and, in particular, study of their transport properties moved into the focus of current research. However, in almost all known 3D TI the dc electron transport is often hindered by the high carrier density in the bulk [4–6]. A promising way to overcome this problem serves the recent progress in growth of the 3D TI applying molecular-beam-epitaxy technique; see, e.g., [7,8]. The existence of TI surface states in such materials has been demonstrated by the angle-resolved photoemission spectroscopy (ARPES) [9–11]. Furthermore, low-temperature electric measurements in thin films and nanowires indicate substantial surface state transport [12–18]. However, the electron transport exclusively determined by surface electrons, in particular, at room temperature, remains a challenge.

Here, we report on the observation and study of a room temperature high frequency transport phenomena solely determined by 2D Dirac fermions in 3D TI. We show that excitation of molecular-beam-epitaxy-grown Sb_2Te_3 and Bi_2Te_3 crystals by terahertz (THz) electric fields results in a photogalvanic effects (PGE): a nonlinear transport effect yielding a dc electric current proportional to the square of the ac electric field [19,20]. A selective excitation of dc current in TI surface states becomes possible due to the specific feature of PGE, whose prerequisite is a lack of inversion center. As these crystals, like most of the 3D TI, are centrosymmetric, this requirement is fulfilled for the surface states only. Because of this "symmetry filtration," the PGE is generated in the surface electron system only, even in the materials with substantial conductance in the bulk. We demonstrate that the PGE is caused by asymmetric scattering of Dirac electrons driven back and forth by the THz field. The effect reflects the surface symmetry and allows one to determine the orientation of the surface domains, to probe high frequency conductivity in TI, and to study tiny details of electron scattering.

Before discussing the experimental results we address the basic physics of the PGE in 3D TI and set requirements to the experimental geometry. The surface states of TI are based on the crystalline structure, see Fig. 1(d), which includes a sequence of five atomic layers, so called a quintuple layer (QL), oriented perpendicularly to the c axis [21]. The point-group symmetry of $(Sb, Bi)_2Te_3$ bulk crystals is D_{3d}, which includes the center of inversion, whereas the *surface* lacks the space inversion and its point group is C_{3v}. The trigonal symmetry of 2D surface carriers makes the elastic scattering asymmetric, giving rise to a dc electric current in response to the ac electric field. The process of current generation is illustrated in Fig. 2 where the scatterers are sketched as randomly distributed but identically oriented wedges lying in the QL plane. In the absence of radiation, the flows of anisotropically scattered electrons exactly compensate for each other. Application of the linearly polarized THz field results in *alignment* of electron momenta: the total number of Dirac electrons driven back and forth by ac electric field $\boldsymbol{E}(t)$ increases while the number of particles moving, e.g., perpendicularly to the field direction, decreases. The corresponding

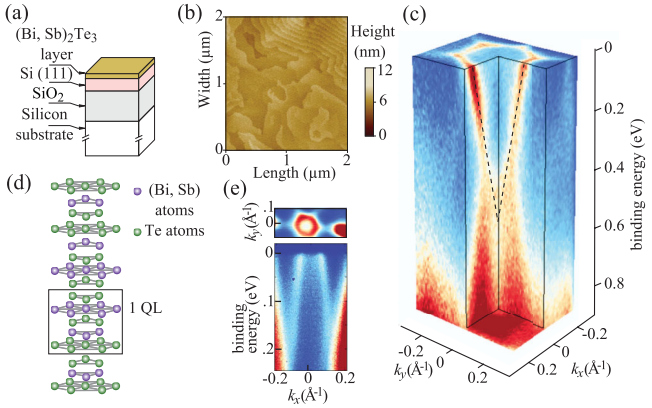

FIG. 1 (color). (a) Sample sketch. (b) AFM surface scan of Sb_2Te_3. (c) and (e) ARPES measurement of p-type Sb_2Te_3 and n-type Bi_2Te_3. (d) Structure of $(Sb, Bi)_2Te_3$ layer.

stationary correction to the electron distribution function scales as a square of the ac electric field magnitude [22]. The alignment of electron momenta itself does not lead to the dc electric current but, due to asymmetric scattering by wedges, the excess of the number of carriers moving along the field violates the balance of the flows [23–25], and the linear PGE current is generated. The resulting current direction depends on the relative orientation of the ac electric field and wedges: e.g., the field parallel to the wedges base, see Fig. 2(a), yields the current flowing in the x_0 direction while rotation of the electric field by 90° reverses the current direction; see Fig. 2(b). Symmetry analysis yields the polarization dependence of the PGE current density $\boldsymbol{j}$:

$$j_{x_0} = \chi(|E_{x_0}|^2 - |E_{y_0}|^2) = -\chi|E_0|^2 \cos 2\alpha_0,$$
$$j_{y_0} = -\chi(E_{x_0}E^*_{y_0} + E_{y_0}E^*_{x_0}) = \chi|E_0|^2 \sin 2\alpha_0. \quad (1)$$

Here, E_0 is the electric field amplitude, the factor χ is the single linearly independent constant, and α_0 is counted anticlockwise from y_0. Note that the brackets in Eqs. (1) divided by $|E_0|^2$ represent the Stokes parameters [26] of the radiation s_1 and s_2, respectively.

In the bulk centrosymmetric $(Sb, Bi)_2Te_3$ crystals spatial inversion forbids the linear coupling between the current and electric field square and, in contrast to the surface, the PGE dc current cannot be generated. This difference has been addressed in Ref. [27], where control over TI photocurrents with light polarization was demonstrated by study of photon helicity-induced (circular) PGE. However, the

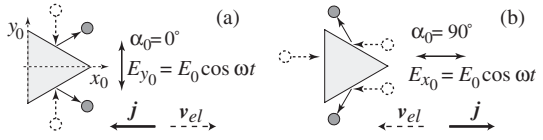

FIG. 2. Model of the PGE excited in surface states of $(Sb, Bi)_2Te_3$ due to asymmetry of elastic scattering by wedges.

strict symmetry filtration is violated due to a possible competing contribution of the photon drag effect [19,20], which does not require the lack of inversion symmetry. While in analysis of Ref. [27] the photon drag effect in the bulk has been ruled out due to its spin degeneracy, most recent observations demonstrated that substantial linear and circular photon drag currents can be efficiently generated even in 2D materials with vanishing spin-orbit coupling, such as graphene, and gives a response comparable with PGE [19,20,28]. A straightforward way to distinguish the PGE response emerging from the surface states and photon drag effect provides experiments with reversed direction of the light propagation. Indeed, while the PGE is determined by the electric field orientation and is insensitive to the radiation propagation direction, the photon drag current being proportional to the photon momentum $\boldsymbol{q}$,

$$j_{x_0} = \mathcal{T}|E_0|^2 q_z s_1, \qquad j_{y_0} = -\mathcal{T}|E_0|^2 q_z s_2, \quad (2)$$

reverses its sign. Here ,$\mathcal{T}$ is the photon drag constant and z is the epilayer c axis, $z \| [0001]$. Note that both types of the photocurrent behave identically upon variation of the radiation polarization state, cf. Eqs. (1) and (2). This indistinguishable behavior is also obtained for linear and circular photocurrents excited at oblique incidence; see Supplemental Material [36]. The straightforward way, however, to separate the surface and the bulk transport is to excite photocurrents, applying the radiation from both sides of the sample.

To explore the high frequency transport in Dirac fermion systems we studied photocurrents excited by THz radiation in Sb_2Te_3 and Bi_2Te_3 grown on Si(111) wafers. A corresponding sketch of the structure is shown in Figs. 1(a) and 1(d) and details of sample growth [8] are given in the Supplemental Material [36]. In Sb_2Te_3 (Bi_2Te_3) samples, the band gap E_g is of the order of 170 (190) meV with the Fermi level referred to the Dirac point $\varepsilon_F \approx 65(100)$ meV and a corresponding Fermi velocity, $v_0 = 4.36 \times 10^5 (4.28 \times 10^5)$ m/s, measured by scanning tunneling spectroscopy and ARPES; see Figs. 1(c),1(e). To measure the current, Ohmic contacts were centered on opposite edges of the squared shaped sample. To apply an ac electric field $\boldsymbol{E}(t)$ in the plane of QL we used a normally incident linearly polarized THz radiation of molecular laser [29–31]; see insets in Fig. 3 and the Supplemental Material [36] for details. The ac field direction was rotated by an azimuth angle α in respect to a sample edge defined as the y axis. The angle of incidence Θ for front and back illuminations were 0° and 180°, respectively.

Exciting samples with the THz electric field we observed a dc current exhibiting a characteristic polarization dependence shown in Fig. 3. Panels (a) and (b) present the photocurrents, $J_x(\alpha)$ and $J_y(\alpha)$, excited by front illumination and measured as a function of the ac electric field orientation. The signals are well fitted by

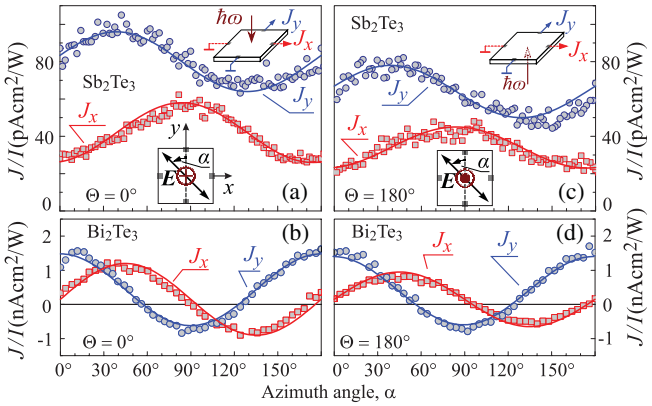

FIG. 3 (color). Normalized photocurrents J_x/I and J_y/I excited with $f = 2.03$ THz for front (left panels) and back (right panels) illumination of the Sb_2Te_3 sample (a),(c) and the Bi_2Te_3 sample (b),(d) at room temperature. Solid lines show fits after Eqs. (3) with phase shifts $3\Phi = -12°$ and 90°, for (a),(c) and (b),(d), respectively. Insets sketch the setups.

$$J_x = [-A(f)\cos(2\alpha - 3\Phi) + C(f)]I,$$
$$J_y = [A(f)\sin(2\alpha - 3\Phi) + C'(f)]I, \qquad (3)$$

where A, C, C', and Φ are fitting parameters, and $I \propto E_0^2$ is the radiation intensity. The photocurrents for the back excitation ($\Theta = 180°$) are shown in Figs. 3(c) and 3(d). As an important result we obtained that the sign of the current as well as its dependence on the azimuth angle α remains unchanged. The same result is obtained for several other samples grown in a similar way (not shown). While in all samples the polarization dependence for front and back illumination remains unchanged, the phase shift, being constant for each sample, varies from 0° to −10°.

Figure 3 shows that besides the offsets C and C' [32], the functional behavior of the photocurrents follows Eqs. (1) and (2) extended by a phase shift and using $\alpha = \alpha_0 + \Phi$. The fact that the sign of the coefficient A remains unchanged at $\boldsymbol{q} \to -\boldsymbol{q}$ inversion unambiguously demonstrates that the photocurrent is dominated by the photogalvanic effect and, consequently, is generated in a 2D Dirac fermion system. Symmetry analysis of the PGE shows that the 3Φ phase shift in the measured photocurrent stems both from the redefinition of the angle α and the fact that the currents J_x and J_y are probed at angle Φ with respect to x_0 and y_0; see the Supplemental Material [36]. Complementary x-ray measurements reveal the threefold symmetry of the surface states and demonstrate the formation of the domains. While two possible types of domains can be formed during $(Sb, Bi)_2Te_3$ growth on the Si (111) substrate, see Fig. 4(a), the x-ray data presented in Fig. 4(b) shows that the majority of the domains have the same orientation with the axis x_0 oriented at the angle Φ to the sample edges. As an important result, the angle $\Phi = -4°$ obtained from the photocurrent measurements in the Sb_2Te_3 sample is equal to that measured in the same sample

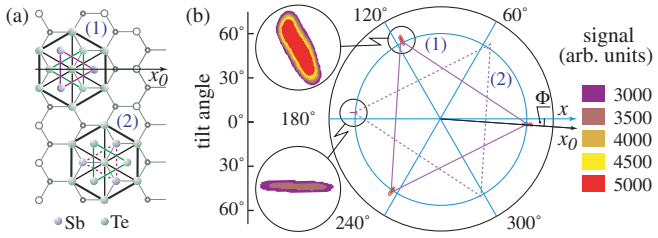

FIG. 4 (color). (a) Two possible domain orientations in Sb_2Te_3 illustrated by solid and dashed violet lines connecting top Sb atoms [7]. (b) X-ray diffraction data obtained for the Sb_2Te_3 sample showing that one domain orientation (highlighted by solid violet lines) dominates. It also reveals that the axis x_0 in this sample is tilted by the angle $\Phi = -4°$ in respect to the sample edge denoted as the x axis.

by x-ray diffraction. This is clearly seen from comparison of Fig. 4(b) and Figs. 3(a) and 3(c), showing the photocurrent for front and back illumination. Moreover, in the Bi_2Te_3 sample with edges oriented along x_0, y_0 axes, as verified by the TEM measurements, the phase shift in the PGE data is 90°; see Figs. 3(b),3(d). Varying the electric field frequency we obtained that the parameter $A(f)$, which determines the photocurrent magnitude, strongly increases with the frequency decrease. Figure 5(c) shows that at low frequencies it closely follows the law $A \propto 1/f^2$. Applying radiation at oblique incidence to the Sb_2Te_3 sample we found that, as expected for the linear PGE considered here, the photocurrent slightly decreases with increasing the angle of incidence $|\Theta|$; see Fig. 5(c).

While the explanation of the photogalvanic effect has been given in a pictorial way above, we resort now to a microscopic description based on the Boltzmann kinetic equation for the electron distribution function $f_{\boldsymbol{p}}(t)$,

$$\frac{\partial f_{\boldsymbol{p}}}{\partial t} + e\boldsymbol{E}\cdot\frac{\partial f_{\boldsymbol{p}}}{\partial \boldsymbol{p}} = -\sum_{\boldsymbol{p}'}(W_{\boldsymbol{p}'\boldsymbol{p}} f_{\boldsymbol{p}} - W_{\boldsymbol{p}\boldsymbol{p}'} f_{\boldsymbol{p}'}), \qquad (4)$$

where the electric field $\boldsymbol{E}(t) = E_0 \exp(-i\omega t) + \text{c.c.}$, and $W_{\boldsymbol{p}'\boldsymbol{p}}$ is a probability for an electron to have the momenta $\boldsymbol{p}$

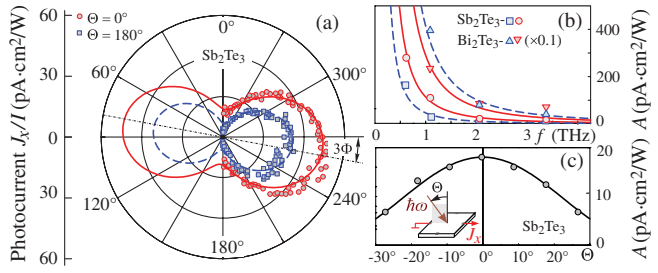

FIG. 5 (color). (a) Photocurrents $J_x(\alpha)/I$ measured in Sb_2Te_3 sample for front and back illumination at $T = 296$ K. Lines are fits after Eqs. (3) with $\Phi = -4°$. Coefficient A as a function of frequency f (b) and the angle Θ (c). Lines in (b) show fits after $A \propto 1/f^2$.

and $\boldsymbol{p}'$ before and after scattering, respectively. Lack of inversion center for the surface electrons makes their elastic scattering asymmetric: even for isotropic scatterers like impurities or phonons, $W_{\boldsymbol{p},\boldsymbol{p}'} \neq W_{-\boldsymbol{p},-\boldsymbol{p}'}$ [23,24]. The probability can be conveniently presented as

$$W_{\boldsymbol{p}',\boldsymbol{p}} = W^{(s)}_{\boldsymbol{p}',\boldsymbol{p}} + W^{(a)}_{\boldsymbol{p}',\boldsymbol{p}}, \tag{5}$$

where $W^{(s)}_{\boldsymbol{p}',\boldsymbol{p}} = W^{(s)}_{-\boldsymbol{p}',-\boldsymbol{p}}$ is the symmetric part, and the scattering asymmetry is described by $W^{(a)}_{\boldsymbol{p}',\boldsymbol{p}} = -W^{(a)}_{-\boldsymbol{p}',-\boldsymbol{p}}$ which is nonzero due to C_{3v} symmetry of the surface states. The absence of backscattering for Dirac fermions is taken into consideration by the standard factor in the symmetrical part [33]: $W^{(s)}_{\boldsymbol{p}',\boldsymbol{p}} \propto \cos^2[(\varphi_{\boldsymbol{p}'} - \varphi_{\boldsymbol{p}})/2]$, where $\varphi_{\boldsymbol{p}}, \varphi_{\boldsymbol{p}'}$ are the polar angles of vectors $\boldsymbol{p}$ and $\boldsymbol{p}'$.

We iterate the kinetic equation in the second order in the field amplitude taking into account that $eE_0 v_0 \tau_{\mathrm{tr}}/\varepsilon_F \ll 1$, where the linear 2D energy dispersion with the velocity v_0 is considered, and the transport scattering time τ_{tr}, determining the mobility of 2D Dirac fermions, is related to the symmetric part of the scattering probability as $\tau_{\mathrm{tr}}^{-1} = \sum_{\boldsymbol{p}'} W^{(s)}_{\boldsymbol{p}',\boldsymbol{p}}[1 - \cos(\varphi_{\boldsymbol{p}'} - \varphi_{\boldsymbol{p}})]$. As a result, we find the stationary correction to the distribution function $\delta f_{\boldsymbol{p}} \propto |E_0|^2$ [22]. Calculating the photocurrent density by the standard expression $\boldsymbol{j} = e\sum_{\boldsymbol{p}} \delta f_{\boldsymbol{p}} v_0 \boldsymbol{p}/p$, we obtain

$$j_{x_0,y_0} = \pm s_{1,2} |E_0|^2 e v_0 \sigma(\omega) \times \left[\frac{1}{\varepsilon_F^2}\frac{d(\Xi\tau_2\varepsilon_F^2)}{d\varepsilon_F} + \frac{1-\omega^2\tau_{\mathrm{tr}}\tau_2}{1+(\omega\tau_2)^2}\frac{\Xi\tau_2\varepsilon_F}{\tau_{\mathrm{tr}}}\frac{d(\tau_{\mathrm{tr}}/\varepsilon_F)}{d\varepsilon_F}\right]. \tag{6}$$

Here, the high-frequency conductivity is given by the Drude expression for degenerate 2D carriers $\sigma(\omega) = e^2\varepsilon_F\tau_{\mathrm{tr}}/[4\pi\hbar^2(1+\omega^2\tau_{\mathrm{tr}}^2)]$, and the currents proportional to $+s_1$ and $-s_2$ correspond to j_{x_0}, j_{y_0}, respectively. The time τ_2 being of the order of τ_{tr} describes relaxation of the above discussed alignment of electron momenta. It is given by $\tau_2^{-1} = \sum_{\boldsymbol{p}'} W^{(s)}_{\boldsymbol{p}',\boldsymbol{p}}[1 - \cos 2(\varphi_{\boldsymbol{p}'} - \varphi_{\boldsymbol{p}})]$. The asymmetry of the scattering probability is taken into account by the factor $\Xi \ll 1$

$$\Xi = \tau_{\mathrm{tr}} \sum_{\boldsymbol{p}'} \langle 2\cos\varphi_{\boldsymbol{p}} \cos 2\varphi_{\boldsymbol{p}'} W^{(a)}_{\boldsymbol{p}',\boldsymbol{p}} \rangle_{\varphi_{\boldsymbol{p}}}, \tag{7}$$

where the brackets denote averaging over the directions of $\boldsymbol{p}$ at the Fermi circle. Note that Eq. (6) agrees with Eqs. (1) obtained from the phenomenological arguments.

The microscopic theory of the PGE presented above describes all major features observed in the experiments. It shows that, in agreement with experimental findings, the dc electric currents probed along and normal to the wedges base are proportional to the square of the ac electric field amplitude $|E_0|^2$, described by one constant $A(f)I = \chi|E_0|^2$ and vary upon rotation of the electric field direction after the Stokes parameters s_1 and s_2, respectively. The theory also describes well the frequency dependence of the photocurrent ($j \propto 1/f^2$); see Fig. 5(b). Indeed, at $\omega\tau_{\mathrm{tr}}, \omega\tau_2 \gg 1$ Eq. (6) yields $j \sim e^3 v_0 \Xi |E_0|^2/(\hbar^2\omega^2)$. A small deviation from this dependence observed at high frequencies, see Fig. 5(b), can be caused by the surface roughness, see Fig. 1(b), which modifies the frequency behavior of $\sigma(\omega)$, like it has been reported for the epitaxial graphene [34] and other multilayer thin film systems, see, e.g., [35]. Equation (6) also reveals that the magnitude of the PGE current, as well as its dependence on the electric field frequency or sample temperature, are determined by the dominant elastic scattering mechanism for Dirac fermions. In particular, the photocurrent can be generated for the scattering by Coulomb impurities or phonons, but vanishes for that by short-range impurities; see the Supplemental Material [36]. Thus, the observation of the PGE in Sb_2Te_3 crystals indicates the dominant role of the Coulomb scattering in the surface state electron transport. Further details of scattering can be obtained from the study of the PGE spectral behavior at $\omega\tau_{\mathrm{tr}} \leq 1$, where the scattering mechanism affects the frequency dependence of the photocurrent (via τ_{tr} and τ_2). Finally, we estimate the PGE magnitude following Eq. (6). We obtain for the radiation of $f = 0.6$ THz focused in the 2.8 mm spot the experimental value $A = 280$ pA cm^2/W for the Sb_2Te_3 sample at the scattering asymmetry factor $\Xi \sim 10^{-5}$. An order of magnitude larger photocurrent for Bi_2Te_3 is explained by a higher Fermi energy in this sample, which yields $\Xi \sim 10^{-4}$ ($\Xi \propto \varepsilon_F^3$, see Supplemental Material [36]).

Finally, we comment on the observed difference in the strength of the photocurrent excited at top and bottom illumination; see Fig. 5(b). First of all, it may come from the unequal photocurrent contributions excited in the top and interfacial surfaces separated by the bulk material, e.g., due to different scattering times or different ratio between the density of domains with two opposite orientations. Together with the radiation absorption in the bulk, this will result in the different value of the photocurrent given by the sum of both contributions. Secondary, in spite of the fact that the photocurrent is dominated by PGE, a small input to the photocurrent may still come from the photon drag effect either in the surface states or bulk. As the sign of the photon drag current depends on the light propagation direction, it will increase or decrease the total photocurrent excited by top and back illumination.

To summarize, the observed photogalvanic effect in the surface states provides an opto-electronic method to selectively excite and study high frequency transport of the Dirac fermions in 3D TI. The photocurrent, being sensitive to the surface symmetry and scattering details, can be applied to map the domain orientation in 3D TI and study

the high frequency conductivity of the surface states even at room temperature. While in the studied frequency range and materials the photoresponse is dominated by PGE, our analysis demonstrates that to ensure that the photoresponse comes from the Dirac fermions and to exclude a possible contribution of the bulk, the experiments with front and back sample excitation are required. And, last but not least, we note that we considered above the photocurrent formed as a result of scattering by impurities or acoustic phonons. However, the effects of strong spin-orbit coupling as well as scattering by the domain boundaries may contribute to the current formation influencing the photocurrent's magnitude.

We thank M. M. Glazov, M. Schmalzbauer, E. L. Ivchenko, and J. H. Bardarson for fruitful discussions. The support from the DFG (SPP 1666), Elite Network of Bavaria (K-NW-2013-247), HGF virtual Institute, RFBR, and EU programme POLAPHEN is gratefully acknowledged.

[1] M. Z. Hasan and C. L. Kane, Rev. Mod. Phys. **82**, 3045 (2010).
[2] J. E. Moore, Nature (London) **464**, 194 (2010).
[3] X. L. Qi and S. C. Zhang, Rev. Mod. Phys. **83**, 1057 (2011).
[4] J. G. Checkelsky, Y. S. Hor, M. H. Liu, D. X. Qu, R. J. Cava, and N. P. Ong, Phys. Rev. Lett. **103**, 246601 (2009).
[5] A. A. Taskin and Y. Ando, Phys. Rev. B **80**, 085303 (2009).
[6] J. G. Analytis, J. H. Chu, Y. Chen, F. Corredor, R. D. McDonald, Z. X. Shen, and I. R. Fisher, Phys. Rev. B **81**, 205407 (2010).
[7] S. Borisova, J. Krumrain, M. Luysberg, G. Mussler, and D. Grützmacher, Cryst. Growth Des. **12**, 6098 (2012).
[8] L. Plucinski, A. Herdt, S. Fahrendorf, G. Bihlmayer, G. Mussler, S. Döring, J. Kampmeier, F. Matthes, D. E. Bürgler, D. Grützmacher, S. Blügel, and C. M. Schneider, J. Appl. Phys. **113**, 053706 (2013).
[9] Y. L. Chen, J. G. Analytis, J. H. Chu, Z. K. Liu, S. K. Mo, X. L. Qi, H. J. Zhang, D. H. Lu, X. Dai, Z. Fang, S. C. Zhang, I. R. Fisher, Z. Hussain, and Z. X. Shen, Science **325**, 178 (2009).
[10] Y. Xia, D. Qian, D. Hsieh, L. Wray, A. Pal, H. Lin, A. Bansil, D. Grauer, Y. S. Hor, R. J. Cava, and M. Z. Hasan, Nat. Phys. **5**, 398 (2009).
[11] D. Hsieh, Y. Xia, D. Qian, L. Wray, J. H. Dil, F. Meier, J. Osterwalder, L. Patthey, J. G. Checkelsky, N. P. Ong, A. V. Fedorov, H. Lin, A. Bansil, D. Grauer, Y. S. Hor, R. J. Cava, and M. Z. Hasan, Nature (London) **460**, 1101 (2009).
[12] J. Chen, H. J. Qin, F. Yang, J. Liu, T. Guan, F. M. Qu, G. H. Zhang, J. R. Shi, X. C. Xie, C. L. Yang, K. H. Wu, Y. Q. Li, and L. Lu, Phys. Rev. Lett. **105**, 176602 (2010).
[13] K. Eto, Z. Ren, A. A. Taskin, K. Segawa, and Y. Ando, Phys. Rev. B **81**, 195309 (2010).
[14] H. Steinberg, D. R. Gardner, Y. S. Lee, and P. Jarillo-Herrero, Nano Lett. **10**, 5032 (2010).
[15] J. G. Analytis, R. D. McDonald, S. C. Riggs, J. H. Chu, G. S. Boebinger, and I. R. Fisher, Nat. Phys. **6**, 960 (2010).
[16] L. B. Zhang, K. Chang, X. C. Xie, H. Buhmann, and L. W. Molenkamp, New J. Phys. **12**, 083058 (2010).
[17] J. G. Checkelsky, Y. S. Hor, R. J. Cava, and N. P. Ong, Phys. Rev. Lett. **106**, 196801 (2011).
[18] J. H. Bardarson and J. E. Moore, Rep. Prog. Phys. **76**, 056501 (2013).
[19] E. L. Ivchenko, *Optical Spectroscopy of Semiconductor Nanostructures* (Alpha Science Int., Harrow, UK, 2005).
[20] S. D. Ganichev and W. Prettl, *Intense Terahertz Excitation of Semiconductors* (Oxford Univ. Press, Oxford, 2006).
[21] H. Zhang, C. X. Liu, X. L. Qi, X. Dai, Z. Fang, and S. C. Zhang, Nat. Phys. **5**, 438 (2009).
[22] The stationary correction to the distribution function $f_{\boldsymbol{p}}(t)$ is obtained by writing it as an expansion in powers of the electric field $f_{\boldsymbol{p}}(t) = f_0 + f_{\boldsymbol{p}}^{(1)}(t) + f_{\boldsymbol{p}}^{(2)}$ with the oscillating in time term $f_{\boldsymbol{p}}^{(1)}(t) \propto \exp(-i\omega t)$ and the stationary term $f_{\boldsymbol{p}}^{(2)} \propto |\boldsymbol{E}|^2$ being *second order* in the electric field.
[23] V. I. Belinicher and B. I. Sturman, Sov. Phys. Usp. **23**, 199 (1980).
[24] B. I. Sturman and V. M. Fridkin, *The Photovoltaic and Photorefractive Effects in Noncentrosymmetric Materials* (Gordon and Breach, Philadelphia, 1992).
[25] W. Weber, L. E. Golub, S. N. Danilov, J. Karch, C. Reitmaier, B. Wittmann, V. V. Bel'kov, E. L. Ivchenko, Z. D. Kvon, N. Q. Vinh, A. F. G. van der Meer, B. Murdin, and S. D. Ganichev, Phys. Rev. B **77**, 245304 (2008).
[26] M. Born and E. Wolf, *Principles of Optics* (Pergamon, Oxford, 1970).
[27] J. W. McIver, D. Hsieh, H. Steinberg, P. Jarillo-Herrero, and N. Gedik, Nat. Nanotechnol. **7**, 96 (2012).
[28] M. M. Glazov and S. D. Ganichev, Phys. Rep. **535**, 101 (2014).
[29] J. Karch, P. Olbrich, M. Schmalzbauer, C. Zoth, C. Brinsteiner, M. Fehrenbacher, U. Wurstbauer, M. M. Glazov, S. A. Tarasenko, E. L. Ivchenko, D. Weiss, J. Eroms, and S. D. Ganichev, Phys. Rev. Lett. **105**, 227402 (2010).
[30] S. D. Ganichev, E. L. Ivchenko, and W. Prettl, Physica (Amsterdam) **14E**, 166 (2002).
[31] E. Ziemann, S. D. Ganichev, I. N. Yassievich, V. I. Perel, and W. Prettl, J. Appl. Phys. **87**, 3843 (2000).
[32] The polarization independent offset may be caused by the nonperfectly flat surface; see the AFM photograph in Fig. 1, which locally reduces the symmetry of the surface states and allows a polarization independent contribution to the photogalvanic effect.
[33] S. Das Sarma, S. Adam, E. H. Hwang, and E. Rossi, Rev. Mod. Phys. **83**, 407 (2011).
[34] I. Crassee, M. Orlita, M. Potemski, A. L. Walter, M. Ostler, Th. Seyller, I. Gaponenko, J. Chen, and A. B. Kuzmenko, Nano Lett. **12**, 2470 (2012).
[35] S. G. Engelbrecht, L. De Angelis, M. Toennies, and R. Kersting, Appl. Phys. A **113**, 641 (2013).
[36] See Supplemental Material at http://link.aps.org/supplemental/10.1103/PhysRevLett.113.096601 for details on the experimental geometry, sample growth and characterisation, theoretical calculation and estimation of the photocurrent.